Chapter 5

Strengthening and hardening behaviour of nanostructured bainitic steel

5.1 Introduction

The strength and ductility of nanostructured bainite come from the strain hardening/work hardening of the material, which is affected by the stability of retained austenite. In this context, the stability of RA is related to its mechanical stability, which refers to its ability to resist the formation of martensite during deformation. The formation of martensite from retained austenite depends on two major factors: carbon content and the morphology of RA [12]. Very high carbon content can lower the deformation-induced martensite start temperature, resulting in the partial transformation of austenite during deformation. Similarly, too low carbon content will increase the martensite start temperature, and early deformation-induced martensite formation can lead to failure [13].

The 25-hour and 48-hour austempered samples are used to observe the carbon content in filmy retained austenite and blocky retained austenite. Additionally, the distribution of carbon and strain from the bainite/austenite interface to the centre of BRA is studied. These two samples are subjected to tensile testing to analyse the different stages of work hardening behaviour and identify the effect of carbon distribution on deformation mechanisms.

5.2. Results

The X-ray diffraction analysis confirms the presence of retained austenite in both austempered samples, as seen in Figure 5.1a. The Rietveld refinement method is employed to analyse the XRD patterns, as shown in Figure 5.1a for the D2-25h and D2-48h samples, respectively. The volume percent of bainite and retained austenite in D2-25h are estimated to be 35±2 % and 65±2 %, respectively. As the austempering time is increased to 48 hours, the volume percent of bainite increases to 54±3 %. The volume percent of FRA and BRA in the D2-25h sample are calculated by deconvoluting and fitting the peaks with a Gaussian function [215–217], as shown in Figure 5.1b. The volume fraction is determined by taking the average

area under the fitted peaks for three different planes of austenite. The volume percent of FRA and BRA in the D2-25h sample is found to be 23±2 % and 42±3 %, respectively. After 48 hours of austempering, the austenite peaks become more symmetric compared to the D2-25h sample due to the homogeneity in carbon distribution, as shown in Figure 5.1c. At the initial stage of transformation, the different carbon content in FRA and BRA causes two different humps in the XRD pattern [217,218] . The hump at the lower angle is due to presence of more carbon content and belong to FRA, whereas the higher angle side contain relatively lower carbon and belong to BRA (Figure 5.1b). Due to difficulty in estimation of blocky and filmy retained austenite for the symmetric peaks, it is calculated using another method described in next sections.

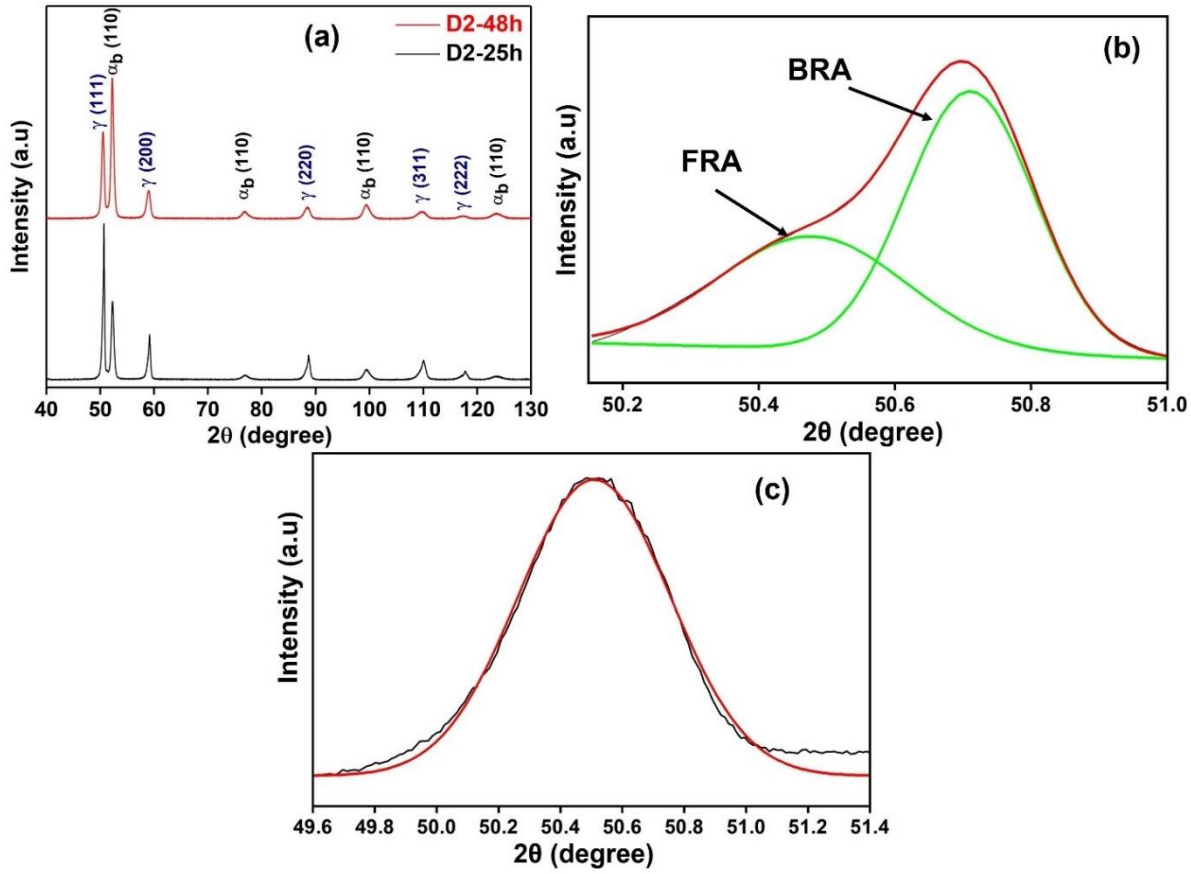

Figure 5.1. *XRD patterns of (a) D2-25h (black colour) and D2-48h (red colour), (b) deconvolution of (111) austenite peaks of D2-25h sample and (c) (111) peak of D2-48h sample showing symmetric peak.*

The lattice parameter of austenite and bainite in the D2-25h sample is found to be 3.619±0.003 Å and 2.876±0.002 Å, respectively. Although the lattice parameter is the average of all the peaks, two different lattice parameters can still be observed in the austenite phase of the D2-25h sample, one for FRA and another for BRA. After austempering for 48 hours, the lattice parameter increases to 3.623±0.002 Å in the austenite phase and decreases to 2.873±0.002 Å in the bainite phase. The increased lattice parameter of retained austenite with increasing austempering time indicates an increase in carbon content, which can be attributed to carbon diffusion from the bainite phase into the retained austenite phase. On the other hand, the decrease in the lattice parameter of bainite with increasing austempering time indicates a reduction in carbon content due to carbon diffusion from the bainite phase into the matrix. The calculated carbon contents in the retained austenite and bainite phases in the D2-25h sample are 1.07±0.03 mass % and 0.21±0.03 mass %, respectively. After austempering for 48 hours, the carbon content in retained austenite increases to 1.15±0.02 mass %, while the carbon content in bainite decreases to 0.12±0.01 mass %.

The dislocation density in both phases is estimated using the MWH method. The dislocation density in the bainite phase of D2-25h is $28x10^{15}/m^2$. However, with further austempering for 48 hours, the dislocation density in bainite decreased marginally to $26x10^{15}/m^2$, while in retained austenite, it decreased significantly from $4.1x10^{15}/m^2$ in the D2-25h sample to $2.2x10^{15}/m^2$ for D2-48h samples.

Figures 5.2a and d show magnified regions of IPF maps with superimposed high-angle grain boundaries (HAGBs) (15°-65°) for the D2-25h and D2-48h samples, respectively. The fraction of HAGBs in the bainite phase of the D2-25h sample is found to be 0.41, which increases to 0.76 after 48 hours of austempering. Similarly, the fraction of HAGBs in the austenite phase of the D2-25h sample is 0.15, which increases to 0.59 in the D2-48h sample. Figures 5.2b and e display the superimposition of geometrically necessary dislocation (GND) maps on IQ maps

in the bainite phase of the D2-25h and D2-48h samples, respectively. The GND density in the bainite phase of the D2-25h sample is 2×10^{14} m^{-2}, but it decreases to 1.2×10^{14} m^{-2} after 48 hours of austempering. Similarly, the GND density in the austenite phase decreases from 1.3×10^{14} m^{-2} in the D2-25h sample to 1×10^{14} m^{-2} in the D2-48h sample. The GND maps of the austenite phase in the D2-25h and D2-48h samples are shown in Figures 5.2c and f, respectively. The GND is primarily present near the bainite/austenite interface, whereas the middle portion of blocky austenite is free from them.

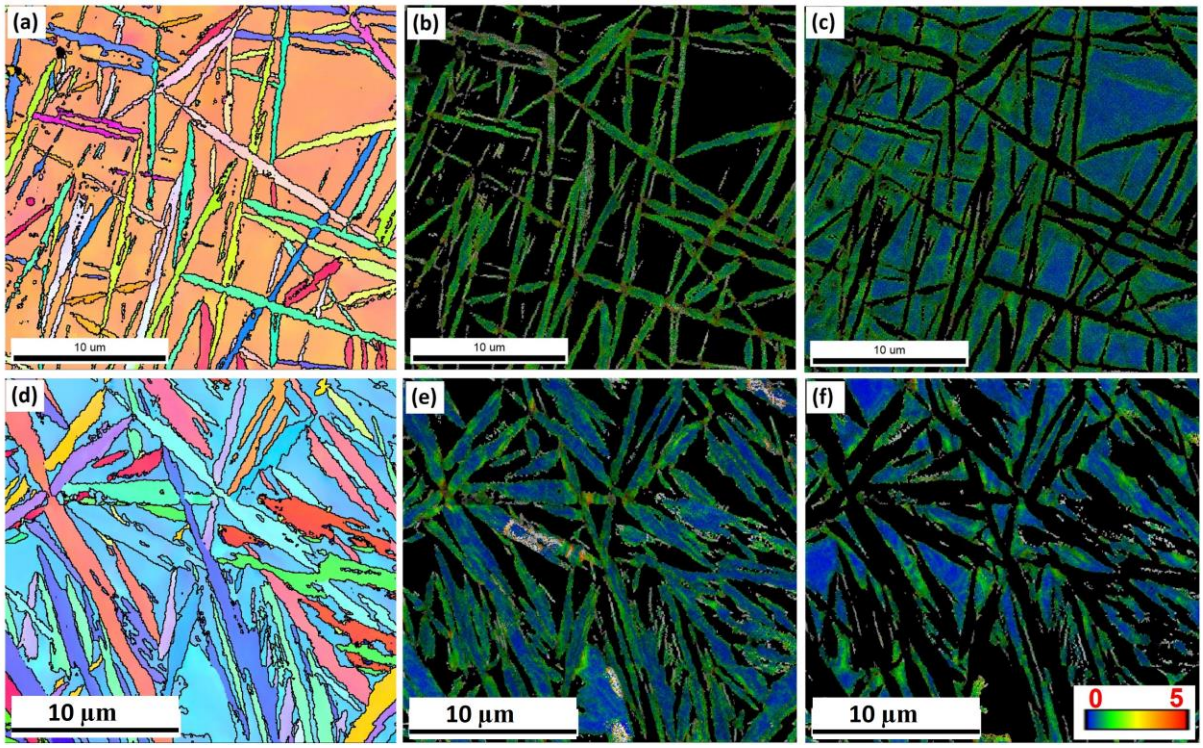

Figure 5.2. *IPF maps along normal direction superimposed with high angle grain boundaries (black colour) (a) D2-25h, (d) D2-48h and GND density superimposed on IQ map in bainite phase (b) D2-25h, (e) D2-48h and in austenite phase (c) D2-25h and (f) D2-48h (misorientation angle of 15°-65° is referred as high angle grain boundaries).*

TEM BF images shown in Figure 5.3 reveal bainite and retained austenite phases. The microstructure of the D2-25h sample (Figure 5.3a) shows the presence of a bainitic sheaf. The dark regions inside the sheaf are filmy retained austenite (FRA), and the brighter regions are bainitic subunits. The microstructure of the D2-48h sample (Figure 5.3b) reveals the presence of nanostructured bainite and retained austenite with plate thickness ranging

between 50 nm and 150 nm. The fraction of BRA and FRA in the D2-48h sample is determined following the method in ref. [102] and found to be 22±4 % and 24±5 % respectively.

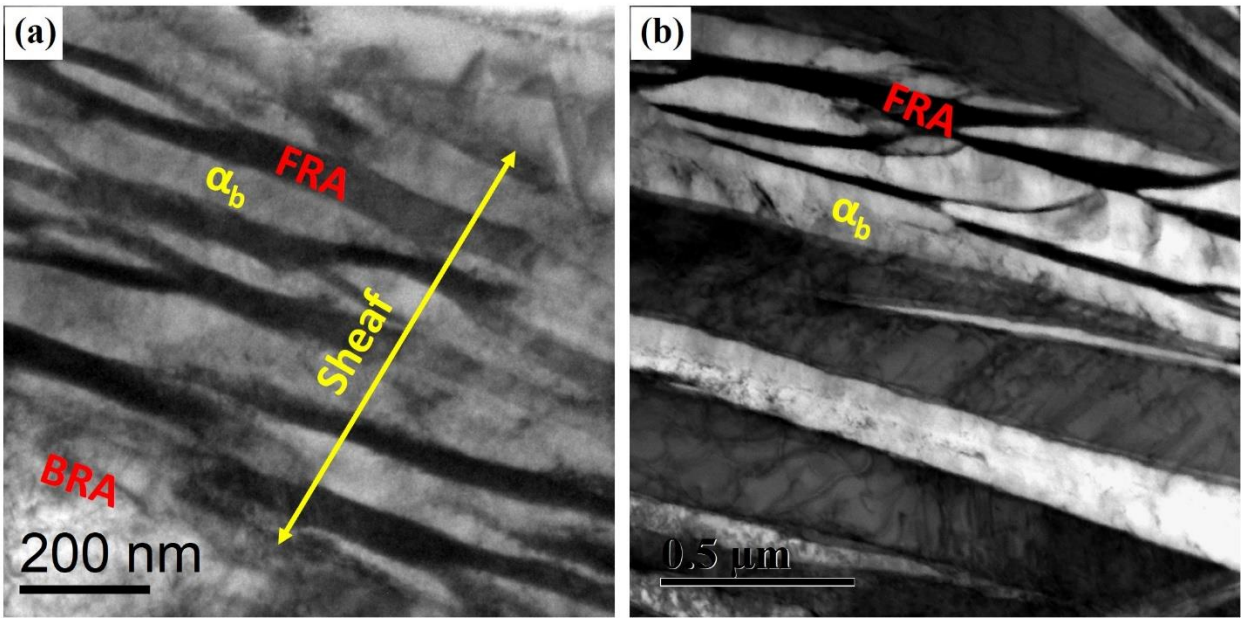

Figure 5.3. *TEM bright-field images of (a) D2-25h and (b) D2-48h samples.*

The engineering stress vs. engineering strain curves for D2-25h and D2-48h samples is shown in Figure 5.4. The yield strength and ultimate tensile strength of D2-25h are reported to be 1092 MPa and 1440 MPa, respectively. This sample exhibits a uniform elongation as well as total elongation of 6% without necking. After 48 hours of austempering, the YS and UTS of D2-48h increase to 1260 MPa and 1611 MPa, respectively. This sample also exhibits a UE of 6% with a marginal gain in TE of 1.7%. The hardness is also increased from 479±14 HV in D2-25h to 633±25 HV after 48 hours of austempering due to additional bainite formation. The tensile toughness of the samples is calculated from the area under the plastic deformation region of engineering stress-strain curve. Table 5.1 summarizes these results for both samples.

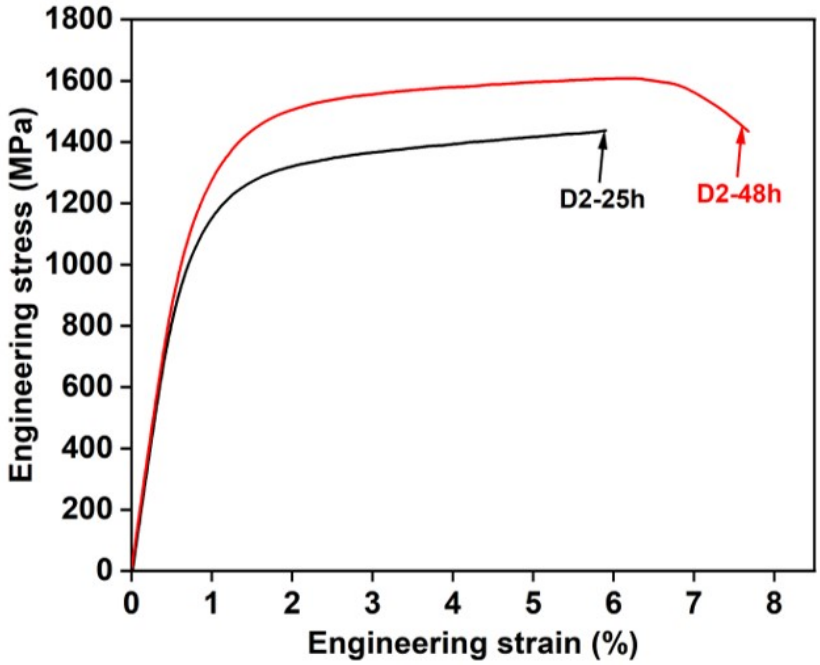

Figure 5.4. *Engineering stress (MPa) vs. strain (%) plots of D2-25h (black) and D2-48h (red) samples.*

Table 5.1. Tensile properties and hardness of the steels after selected austempering treatments.

Sample	YS (MPa)	UTS (MPa)	UE (%)	TE (%)	Toughness (MJ/m^3)	Hardness (HV)
D2-25h	1092	1440	6	6	86.4	479±14
D2-48h	1260	1611	6.24	7.7	100.5	633±25

The true plastic stress-true plastic strain curves are fitted using various work hardening models (Figure 5.5 (a, b)). The fundamental equation that describes work hardening for a single slope is given by Hollomon [164]. The Ludwik equation may better fit metals with variable yield strength and work-hardening behaviour [165]. Materials with pre-strain are typically fitted with the Swift model [166], while the Voce model is used for materials with saturation stress [179]. The work-hardening behaviour of FCC metals with low stacking fault energy is elucidated by the Ludwigson equation [168].

Among the different work hardening models, the Swift equation provides the best fit due to pre-straining of the austenite phase by the bainite plates during transformation. The R-square values in this fitting are 0.997 and 0.995, and the reduced chi-square values are 10.2 and 47 for the D2-25h and D2-48h samples, respectively (Table 5.2). The strength coefficients of strength and pre-strain value of the D2-25h sample are 1932, and 0.0008, respectively. After austempering for 48 hours, the coefficient of strength and amount of pre-strain increase to 2104 and 0.001, respectively, but the work hardening exponent decreases marginally.

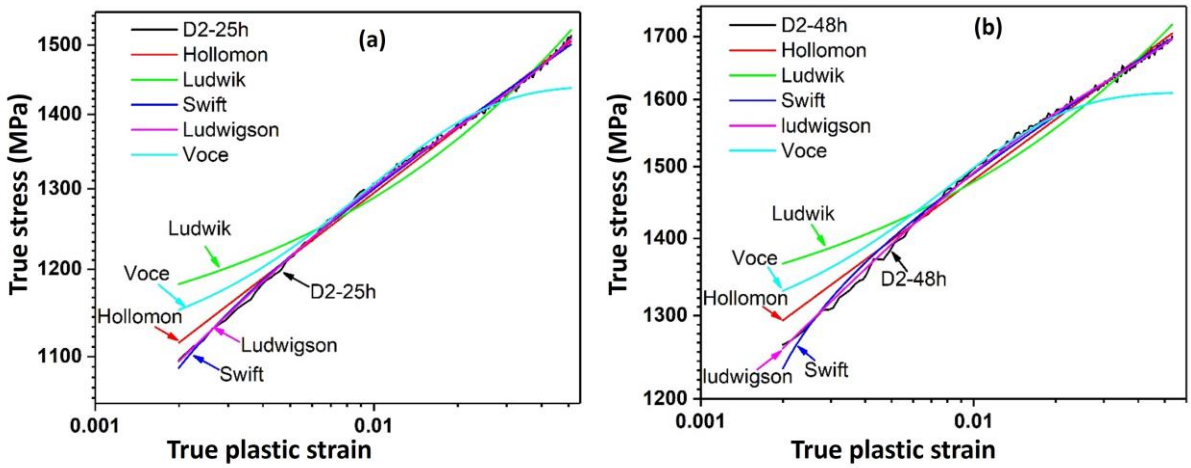

Figure 5.5. *True plastic stress- true plastic strain plots, (a) D2-25h (b) D2-48h fitted with different work hardening equations.*

Table 5.2. Fitting parameters of the Swift model

Sample	K, MPa	N	ε_0	$\chi 2$	R^2
D2-25h	1932	0.08	0.0008	10.2	0.997
D2-48h	2104	0.07	0.001	47	0.995

The logarithmic work hardening rate is plotted against the logarithmic true plastic strain to observe the instantaneous deformation mechanism at different strain levels (Figure 5.6a). In the D2-25h sample, the work-hardening behaviour reveals two stages, followed by a transition stage for the onset of recovery. Straining begins with a short stage I, followed by a wide stage II. There is a very short transition stage at the end of stage II. Work-hardening stage I completes

at a true strain (ε_I) of 0.0056, and Stage II finishes at a true strain (ε_{II}) of 0.0245. The work-hardening behaviour of the D2-48h sample displays three stages, including a transition stage (Tr) between stages II and III. Stage I completes at a true strain (ε_I) of 0.0056, and stage II finishes at a true strain (ε_{II}) of 0.038. Stage III begins at a true strain (ε_{III}) of 0.047 and continues until necking at a true strain of 0.05. Different stages of work hardening are also depicted in the true stress-true strain curves, and the regions of slope change are shown in Fig. 5.6b for both samples.

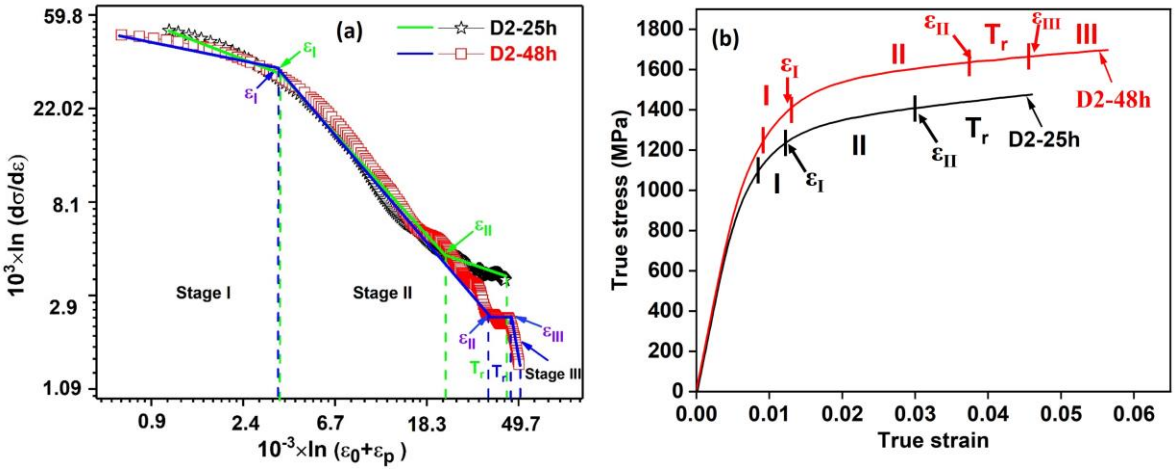

Figure 5.6. *(a) Logarithm work hardening rate vs. logarithm (pre-strain+true plastic strain) plots showing different stages of work hardening and (b) true stress vs true strain plots of D2-25h (black) and D2-48h (red) samples displaying work hardening stages.*

5.3. Discussion

5.3.1 Distribution of carbon and dislocations in RA

The amount of bainite formed after 48 hours of transformation is only 54%, which indicates slower kinetics compared to the D2-25h sample, where 35% bainite is formed after 25 hours of austempering. The enrichment of carbon in the retained austenite phase plays a major role in reducing the rate of transformation [188]. It can be observed from the XRD peaks that carbon is distributed inhomogeneously in the RA phase of the D2-25h sample but more homogeneously in the D2-48h sample (Figure 5.1) due to the longer holding time. The presence

of a high density of dislocations in bainite can be attributed to shape deformation during the phase change process as well as the plastic accommodation of bainitic plates by the retained austenite phase, resulting in a large number of dislocations being generated in the retained austenite phase [82]. However, it is observed that the calculated dislocation density using the MWH method and the EBSD GND map show lower values in both the austenite and bainite phases of the D2-48h sample compared to the D2-25h sample. This can be explained by the fact that a lower transformation rate and longer transformation time can lead to the annihilation of some dislocations, as reported earlier [204,219]. Geometrically necessary dislocations are mostly created near the bainite/austenite interface to accommodate shape strain [220]. The quantity of GND is significantly reduced after 48 hours of transformation, signifying signifying annihilation of dislocation.

5.3.2 Major factors contributing yield strength

The Hall-Petch equation cannot accurately predict the strength of nanostructured materials because pile-up is not possible on a slip plane for grain sizes less than 1 µm. In these materials, yielding occurs through the expansion of dislocation loops [117]. The yield strength of nano-bainitic steel (σ_0) is mainly contributed by nano-sized plates, and it is correlated with the dislocation density in bainite using Equation 1.5 [221,222] as given earlier.

$$\sigma_0 = \sigma_{Fe} + \sigma_{ss} + \sigma_c + k_p(t_b)^{-1} + 7.34 \times 10^{-6}\rho^{1/2} \qquad (5.1)$$

Where σ_{Fe} is the frictional strength (MPa) of pure iron in the annealed condition, σ_{ss} is the substitutional solid solution strengthening (MPa), σ_c is the strengthening contribution (MPa) due to carbon, k_p is a fitting parameter whose value is calculated to be 115 MN/m [102]. The units of t_b and ρ are in m and $\frac{1}{m^2}$, respectively. The coefficient or multiplying factor of dislocation density is having dimension of MN/m. Among these factors, the mean thickness of bainite plates and dislocation density in bainite significantly contribute to strengthening [83].

The plate thickness is inversely related to strength [117], while the dislocation density is directly related [75]. The calculated contribution to strengthening from dislocation density is 324 MPa and 363 MPa for the 25 hours and 48 hours samples, respectively. On the other hand, the contribution from plate thickness is 503 MPa and 608 MPa for the D2-25h and D2-48h samples, respectively. Due to the higher volume fraction of bainite in the D2-48h sample, its yield strength and hardness are higher compared to the D2-25h sample.

5.3.3 Effect of carbon distribution in RA on work hardening behaviour

The strength of bainitic steel is primarily influenced by the volume fraction and thickness of the bainite phase, while the amount of austenite, the carbon content in it, and its morphology affect ductility [124,223]. Since austenite is a ductile phase, it contributes to the overall ductility of the material. A gradual transformation of austenite into martensite leads to higher ductility due to transformation-induced plasticity (TRIP) compared to a faster transformation rate [224]. However, filmy retained austenite, having higher carbon content and isolated due to surrounding bainite, cannot transform to martensite easily. Therefore, it rarely contributes to the ductility of the material through the TRIP process [82,121]. The blocky retained austenite contributes to ductility, depending on the rate of martensitic transformation, which indirectly depends on the alloy content and strain distribution in austenite [121,123]. The D2-25h sample has 42±3 % BRA and 23±2 % filmy retained austenite, whereas austempering for 48 hours increases FRA content to 24±5 % and decreases BRA to 22±4 %. The asymmetric XRD peak of the D2-25h sample indicates inhomogeneous carbon distribution in RA (Figure 5.1b), resulting in non-uniform strain-induced martensite within BRA. Consequently, austenite becomes discontinuous, which leads to a lack of percolation of ductile blocky austenite. In contrast, the D2-48h transformed sample shows a symmetric peak, signifying homogeneous carbon distribution. Although the D2-25h

sample has more RA than the D2-48h sample, higher ductility and more profound necking are observed in the D2-48h sample.

X-ray analysis of the fractured surface of the tensile-tested samples indicates a reduction in the intensity of the austenite phase (Figure 5.7). Examination of the XRD patterns of the tested samples shows the presence of retained austenite of 46±2% and 23±2% in D2-25h and D2-48h, respectively. These findings suggest a partial conversion of blocky retained austenite into strain-induced martensite. The D2-25h sample contains more blocky austenite but less carbon, resulting in mechanically unstable austenite. As a result, when the sample is subjected to tensile loading, a portion of the blocky retained austenite transforms early into brittle martensite, leading to failure at ultimate tensile strength without necking. In contrast, the D2-48h sample contains approximately 1.14 mass % carbon in the RA phase, and non-asymmetric peaks in the XRD patterns of austenite confirm that the carbon distribution is nearly homogeneous. The delayed transformation of higher carbon homogeneous blocky austenite shifts the necking to a larger strain, contributing to ductility due to transformation-induced plasticity. The D2-48h sample exhibits significant tetragonality, with a c/a ratio 1.01 due to a higher level of austenite transformation into martensite. In contrast, the D2-25h sample does not display an additional tetragonal peak.

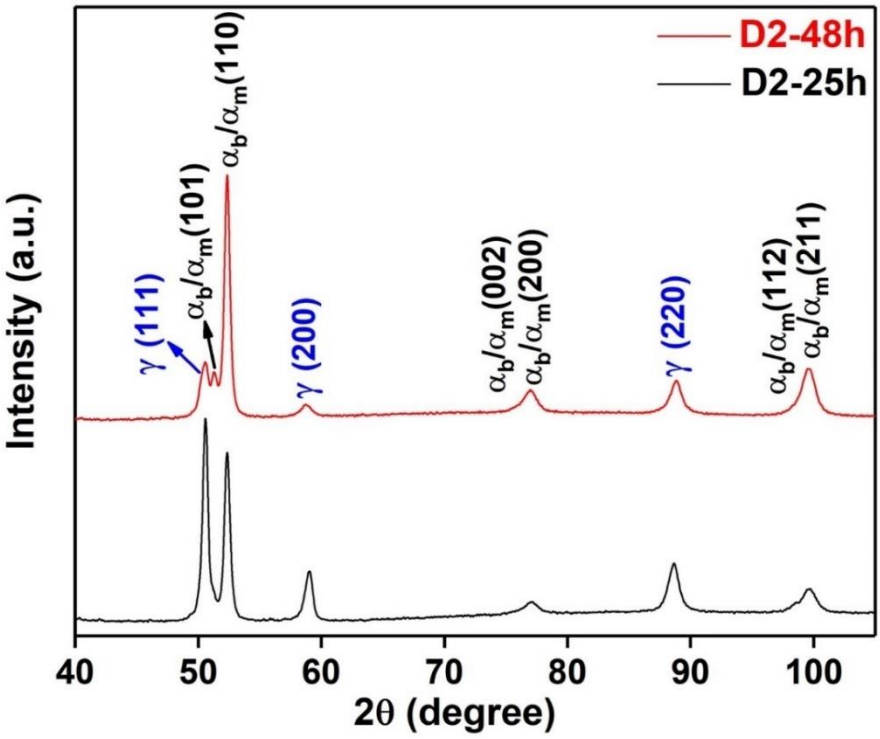

Figure 5.7. *XRD patterns of tensile tested samples.*

5.3.4 Work hardening mechanism

The RA fraction that forms after bainitic transformation can be converted into martensite during uniaxial loading. This transformation can be assisted by stress or induced by strain, depending on the alloying elements present in the RA and its morphology. Martensite transformation after yielding is known as strain-induced transformation, whereas transformation before yielding is known as stress-induced martensitic transformation [111,225]. If the RA is both chemically and mechanically stable, then deformation proceeds by the gliding of mobile dislocations (i.e., homogeneous deformation of work hardening stage I) [128]. Both samples display a short stage I of work hardening. At higher strain (in stage II), mechanically unstable austenite transforms to martensite due to strain-induced martensitic transformation [128]. Although the transition from stage I to stage II occurs at the same true strain, stage II is prolonged to a higher true strain in the D2-48h sample compared to the D2-25h sample. The highest work hardening is observed in this stage due to strain-induced

martensitic transformation of softer RA phases. Most of the BRA and some FRA are gradually converted into martensite (Figure 5.6a). The stage II of the D2-25h sample is shorter because of the more mechanically unstable lesser carbon-containing blocky austenite in the previous case. The blocky austenite is also inhomogeneous in carbon distribution due to shorter austempering times. The non-uniform blocky austenite transforms to martensite at a lesser imposed strain and moves toward the transition stage. But lesser blocky austenite of higher carbon content and better homogeneity in its distribution in the sample of higher austempering time (D2-48h) helps in delayed stage II. In the transition stage (Tr), RA and bainite are deformed simultaneously. The D2-25h sample does not show stage III, unlike the D2-48h sample. In stage III, recovery occurs by the cross-slip of some screw dislocations and the creation of cell structures, leading to a sudden decrease in the work hardening rate. Although both materials show almost a similar amount of work hardening, as the yield strength of the D2-48h sample is much higher than that of the D2-25h one because of the high-volume fraction of bainite, the former report higher UTS.

A schematic diagram in Figure 5.8 illustrates the effect of carbon distribution on work hardening in early stage (D2-25h) and later stage (D2-48h) transformed samples. In the D2-25h sample (Figure 5.8a), the inhomogeneous carbon distribution leads to deformation-induced martensite formation at the centre of blocky retained austenite, with low carbon concentration. However, the regions near bainite plates with high carbon concentrations will not form any martensite. So, localized martensite formation will lead to higher stress concentration at the centre, and cracks will propagate easily through the hard martensite phase [226,227]. In the D2-48h sample (Figure 5.8b), deformation-induced martensite formation will be uniform throughout the blocky austenite due to the homogeneous distribution of carbon. For better ductility, the distribution of austenite should be continuous, as explained earlier [228]. Unlike

the D2-25h sample, stress concentration in the D2-48h sample will be uniform, and the retained austenite in between martensite will act as a load-bearing phase, resulting in higher ductility.

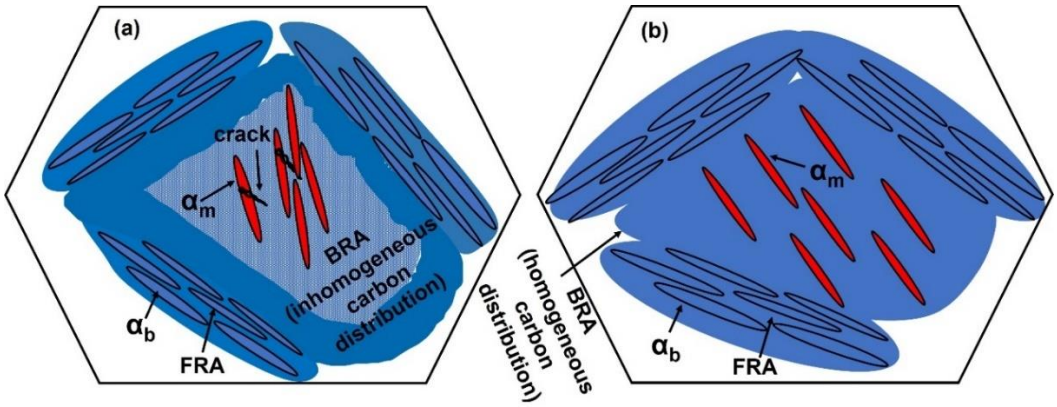

Figure 5.8. *A schematic showing microstructural changes after stage II of work hardening in (a) D2-25h and (b) D2-48h samples (The light blue regions represent low carbon concentration, while the deep blue regions represent high carbon concentration).*

5.4 Conclusions

Austempering of the designed alloy produced nanobainite with a high amount of retained austenite. Microstructural analysis and evaluation of mechanical properties lead to the following conclusions.

- The inhomogeneity in carbon distribution within blocky retained austenite in the D2-25h sample promotes early strain-induced martensitic transformation. This phenomenon has an adverse effect on elongation due to the discontinuity created in the ductile austenite phase.
- The deformation of homogeneous high carbon austenite in the D2-48h sample results in a gradual strain-induced martensitic transformation. This transformation contributes to ductility enhancement due to the transformation-induced plasticity effect.
- The analysis of the tensile fractured sample indicates a large volume fraction of tetragonal martensite (c/a=1.01) in the D2-48h sample due to the conversion of a higher fraction of retained austenite into martensite.